Imaging Enabled Platforms for Development of Therapeutics

Jonathan P. Celli[a], Imran Rizvi[a,d], Adam R. Blanden[a,b], Conor L. Evans[a], Adnan O. Abu-Yousif[a], Bryan Q. Spring[a], Alona Muzikansky[c], Brian W. Pogue[d], Dianne M. Finkelstein[c], Tayyaba Hasan[a]

[a]Wellman Center for Photomedicine, Harvard Medical School, Massachusetts General Hospital, 55 Fruit St, Boston, MA, USA 02114
[b]State University of New York, Binghamton, NY, USA 13902
[c]Biostatistics Center, Massachusetts General Hospital, Boston, MA, USA 02114
[d]Thayer School of Engineering, Dartmouth College, Hanover, NH, USA 03755

ABSTRACT

Advances in imaging and spectroscopic technologies have enabled the optimization of many therapeutic modalities in cancer and noncancer pathologies either by earlier disease detection or by allowing therapy monitoring. Amongst the therapeutic options benefiting from developments in imaging technologies, photodynamic therapy (PDT) is exceptional. PDT is a photochemistry-based therapeutic approach where a light-sensitive molecule (photosensitizer) is activated with light of appropriate energy (wavelength) to produce reactive molecular species such as free radicals and singlet oxygen. These molecular entities then react with biological targets such as DNA, membranes and other cellular components to impair their function and lead to eventual cell and tissue death. Development of PDT-based imaging also provides a platform for rapid screening of new therapeutics in novel in vitro models prior to expensive and labor-intensive animal studies. In this study we demonstrate how an imaging platform can be used for strategizing a novel combination treatment strategy for multifocal ovarian cancer. Using an in vitro 3D model for micrometastatic ovarian cancer in conjunction with quantitative imaging we examine dose and scheduling strategies for PDT in combination with carboplatin, a chemotherapeutic agent presently in clinical use for management of this deadly form of cancer.

Keywords: Photodynamic Therapy, Imaging, 3D Tumor Models, carboplatin, combination treatment, benzoporphyrin derivative monoacid ring A (BPD-MA)

*Corresponding author: thasan@partners.org

1.   INTRODUCTION

Photodynamic Therapy (PDT) is a photochemistry based treatment modality which has received regulatory approvals worldwide for cancer and non cancer pathologies. PDT involves the delivery of a light-activatable chemical, photosensitizer (PS) typically with red light to generate active molecular species such as free radicals and singlet oxygen. These reactive molecules then react with biological targets in cells and tissues to produce cell death and tissue destruction. The basic concepts underlying the photochemical and photophysical processes in PDT and the related energy level diagram depicting the relaxation pathways are shown in Figure 1.

For a PS to be effective as a PDT agent, it needs to have reasonable triplet quantum yields and triplet lifetimes the first excited singlet state S_1 intersystem crosses to the triplet sate T_1 which can react with biological targets directly or, as is believed to be case with PS in clinical use or in preclinical development, T_1 undergoes energy transfer to surrounding oxygen molecules to produce the energized singlet oxygen species. Most PDT relevant PSs which are primarily porphyrinoids have triplet quantum yields in the range of 0.4 to 0.9 and fortunately, fluorescence decay is also a finite relaxation pathway for these PDT agents. This provides the opportunity of using the same molecule as a therapeutic and also as an imaging contrast agent thereby allowing for diagnostic and therapy response monitoring using optical imaging [1]. This is a very exciting area in PDT research and application and image-guidance of surgical resection with PDT agents is now approved for bladder cancer and is being actively developed for brain cancer to help define margins of resection.

Figure 1. A) Perrin-Jablonski energy diagram for a photosensitizer (PS) molecule. After excitation to the singlet excited state the PS may either decay back to the ground state (by fluorescence emission or non-radiative decay) or undergo intersystem crossing to the triplet excited state. From the triplet state the PS may undergo excited state reactions to generate cytotoxic species such as singlet molecular oxygen. PS fluorescence and phosphorescence may be used to image PS localization in tissue and time-resolved imaging techniques may be applied to monitor PS interactions with its microenvironment. **B)** A schematic representation of the interactions of the photosensitizer with either a biological substrate or ground state triplet oxygen in the so-called Type I and Type II photochemical pathways for generation cytotoxic species

In the context of cancer treatments, it is generally thought that the complexity of the disease makes the likelihood of any single treatment being effective in the longterm extremely low. Multiple cellular pathways regulate cancer cell growth and survival [2-6]. It is also well established that all primary treatments such as chemotherapy, radiation therapy and even surgery, elicit cellular responses that may mitigate the effectiveness of primary therapy in the longterm [7, 8]. A classic example of this is the upregulation of vascular endothelial growth factor (VEGF) following radiation, hyperthermia and chemotherapy [9, 10]. All these factors make it critical that appropriate combination therapies with one of more agents be delivered in the right order at the right time. Even when mechanisms are well understood and rational combinations can be proposed, establishing the optimal timing, dose and the order of administration become inadequate or cumbersome to evaluate in the existing systems. Monolayers of cell in culture are too simplistic missing the architectural cues of tumors, which are 3 dimensional (3D) structures, and animal models are expensive and labor intensive with host responses that can be misleading. There is also the problem of the myriad possibilities of even rational combinations so that there is a critical unmet need for systems that can rapidly and reproducibly evaluate treatment response to a host of therapeutic options. Toward that goal, we have developed system that incorporates 3D tumor models and reproducible high throughput, image-based analysis that could efficiently provide guidance for the development of new therapeutics. Here we exemplify how imaging could guide strategies in the design of therapeutic regimens. We have developed a 3D model of ovarian cancer nodules to mimic micrometastatic disease and then use our recently developed robust image-analysis based approach to establish the order of administration of two treatments, PDT and carboplatin [11, 12]. PDT is emerging as a possible option for treating ovarian cancer while carboplatin is one of the standard chemotherapy regimens used in the treatment of this disease with dismal survival statistics [8].

2. MATERIALS AND METHODS

Three-Dimensional Cell Culture. Arrays of three-dimensional tumor nodules were grown in black walled multiwell plates as described in detail by Rizvi et al [12]. Briefly, NIH:OVCAR-5 cells in single cell suspension were grown on beds of Growth Factor Reduced (GFR) Matrigel in blackwalled 24-well dishes (Genetix, New Milton, Hamphsire, UK). 3D cultures were grown in complete growth medium with 2% GFR Matrigel. Recent additional developments extending the disease model to include heterotypic cell-cell interactions as discussed in paper number 7886-8 of these proceedings.

High-content quantitative imaging for characterization of reproducible growth and analysis of cytotoxic response. We use a set of custom developed quantitative image-processing routines for analysis of in vitro growth properties and quantification of cytotoxic response based on methods previously described by Celli et al [11] and recently enhanced and improved as discussed in paper number 7886-7 of these proceedings. Briefly, size characterization to confirm reproducible growth properties was conducted on sets of darkfield microscopy data obtained at regular time intervals from multiple replicates for each 3D culture plating. Size distributions were obtained by a high throughput batch analysis procedure consisting of thresholding and segmentation to identify individual acini. In this manner statistical analysis was performed on data sets consisting of thousands of individual 3D nodules.

Following therapeutic interventions (see below), cultures were incubated with calcein and ethidium bromide fluorescent dyes (Invitrogen, Carlsbad, CA, USA) staining live and dead cells respectively, and images were rapidly acquired across all treatment groups using an Olympus FV-1000 confocal microscope with an automated programmable XY positioning stage [11, 12]. Fluorescence image data sets were stored for offline image analysis providing multiple quantitative metrics for therapeutic outcome based on analysis of fluorescence intensities from live and dead cells and automated segmentation to look at large statistical distributions of nodule-by-nodule response. Briefly, treatment response in this study is described in terms of: 1.) Tumor viability, a ratiometric quantification of the viability of the residual nodules, 2.) Residual tumor volume, a measure of how much viable disease remains on each plate, and 3) Disruption fraction, or D_{frac}, the extent of nodular disruption quantified by the fractional shift in the size distribution due to fragmentation of larger nodules into smaller nodules or single cells. Overall viability was quantified by the ratio of calcein to total fluorescence intensity (calcein plus ethidium) and normalized to no-treatment as previously described. To determine residual volume, calcein images were segmented (as above) to calculate nodule volumes from equivalent

diameters, d_{eq}, by, $V = \frac{4}{3}\pi\left(\frac{d_{eq}}{2}\right)^3$ and then summed to determine total volume reported as fraction of the no-treatment

control. D_{frac} values are calculated by fitting size distributions of residual nodules to a bimodal lognormal form (as previously characterized [11]) for each treatment group and calculating the fractional shift in population of the large mode to the small mode. This analysis is discussed further in paper 7886-7.

Photodynamic Therapy, Carboplatin and Combination Treatments. Cultures were incubated with 250nM BPD-MA for 90 minutes (or Verteporfin, QLT, Inc., Vancouver, BC, Canada) in complete culture media. Immediately prior to irradiation the BPD-MA media was replaced with culture medium containing 2% GFR Matrigel. Each well of the 24-well plate was irradiated with a 690nm fiber coupled diode laser (Model 7401; High Power Devices, Inc., North Brunswick, NJ, USA). Irradiation times were calculated to achieve the desired total fluence at a rate of 40mW/cm^2. All control samples were subjected to the same media changes and sham manipulations as the treatment groups. After PDT cultures were returned to the incubator for 24 hours prior to assessment of treatment response.

Carboplatin treatments were performed by incubating 3D cultures with carboplatin in complete culture medium containing 2% GFR Matrigel for a total of 96 hours. The carboplatin media was refreshed at 48 hours. All control samples were subjected to the same media changes and sham manipulations as the treatment groups. Treatment response was assessed immediately after removal of carboplatin media following the 96-hour incubation, as described above.

Combination treatments were conducted in the same manner as for each montherapy as described above for either BPD-PDT at day 10 followed immediately by carboplatin incubation or for the reverse sequence as discussed in the Results below. In the case of the sequence involving administration of carbo prior to PDT it was necessary to conduct treatment evaluation at day 15 to allow 24 hours for PDT treatment effects to take place.

Multiphoton Fluorescence Imaging of 3D cultures. To characterize 3D multicellular nodules Images were acquired using an inverted Olympus FV1000-MPE (multi photon excitation) microscope equipped with Spectra-Physics DeepSee Ti:Sapphire laser tuned to 750 nm to excite endogenous fluorescence in 3D micronodules. A 40× water immersion objective was used to acquire images. 3D volumes were collected by acquiring depth stacks in 2-μm steps. Two non-descanned detectors collected the autofluorescence emission at 440–490 nm and 510–550 nm respectively. 3D renderings were produced in Imaris Bitplane software. Multiphoton image data was smoothed with a 2-pixel Gaussian filter.

3. RESULTS AND DISCUSSION

The sequence of figures below demonstrate the key features of image-guided therapeutics developed in this paper. Figure 2 establishes that nodular nature of the 3D structures resembling ovarian cancer metastatic disease. The particular nodule depicted is approximately 100 um, and was imaged on day 10 after plating. The nodules grow to larger sizes at longer times and start to exhibit necrosis at these larger dimensions.
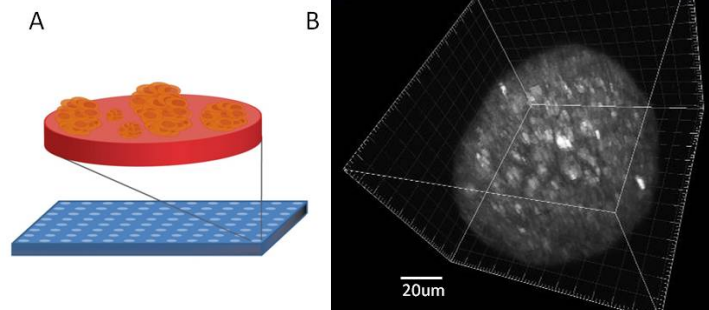

Figure 2: A) Schematic of 3D ovarian tumor arrays and B) a 3D rendering of a representative nodule imaged by multiphoton fluorescence excitation at 759nm.

A critical need in the development of new models and analyses is the reproducibility and Figure 3 demonstrates that the size distribution of nodules in our tumor arrays. This feature of reproducibility is key to validity of the use of our model for guidance of therapy or understanding of mechnisms. The reproducibility within each culture well across independent platings and in separate investigators hands and represent thousands of nodules justified their use in further experiments.
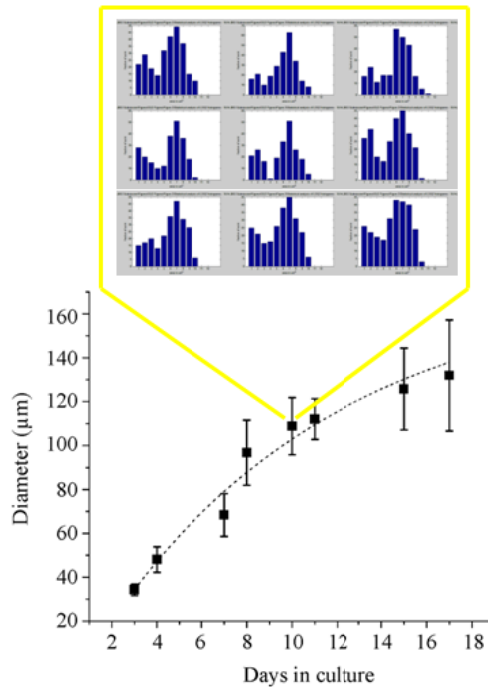
Figure 3: Characterization of reproducibility in 3D tumor arrays. Lower plot shows reproducibility of mean nodule diameters independently calculated from multiple replicates across three separate culture batches at each time point. The blowout shows log-normal histograms (log$_2$ spaced bins from 200 to 409,600 um^2) for size distributions of 9 representative replicates at a given time point (day 10) showing minimal variation in the characteristic bimodal shape which appears within each culture well across independent platings and in separate investigators hands.

Having established the reliability of our 3D model of ovarian cancer nodules, we tested therapies of carboplatin and PDT individually. This was necessary to establish what order of administration of the two treatments might be most beneficial to patients. Figures 4 and 5 show that treatment with even the highest dose of carboplatin produces a ring of death (red) and leaves a core of living cells (green). In contrast, PDT kills cells somewhat more randomly and appears to fragment the nodular structure.
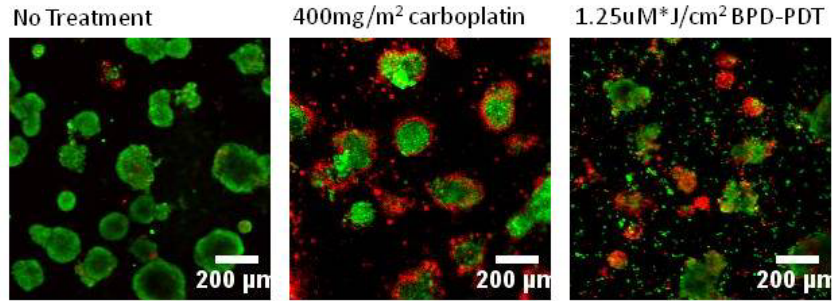
Figure 4: Images of 3D micronodules stained with calcein (green) and ethidium bromide (red) showing live and dead cells respectively, showing contrasting patterns of cytotoxic response from carboplatin and BPD-PDT treatments. In displayed images, contrast was enhanced using hi-lo lookup table, though all quantitative analysis was performed on raw image data.

Further evidence of the characteristic pattern of peripheral cytotoxicity associated with carboplatin treated 3D nodules is shown in Figure 5, which is simply a separation of the two fluorescent channels from the central panel is Figure 4. Figure 5A highlights the residual viable regions at the centers of nodules while in 5B, the halos of red fluorescence
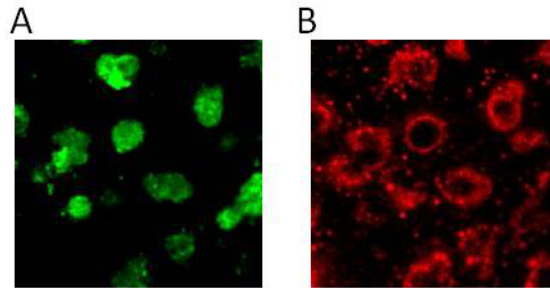
Figure 5: Detail of carboplatin response for the same nodules shown in Figure 2 (center). Separation of the channels highlights **A**, the residual viable cores (green), and **B**, characteristic 'rings' of killing at the periphery of nodules (red).

There are thousands of nodules that undergo the above treatments. In order to extract meaningful data from these observations, it was necessary to establish a quantitative basis of this fragmentation pattern presented in Figure 6. To quantify the observation that PDT disrupts nodular structure shifting the distribution towards smaller sizes we report disruption fraction (D_{frac}) as the fractional shift from the larger size mode to the smaller mode in each bimodal lognormal distribution. As seen in Figure 6D, D_{frac} increases in a dose dependent manner for BPD-PDT, while in Figure 6E, the peripheral pattern of cyototoxic response from carbo produces negligible nodular fragmentation, even at doses up to 10mM.
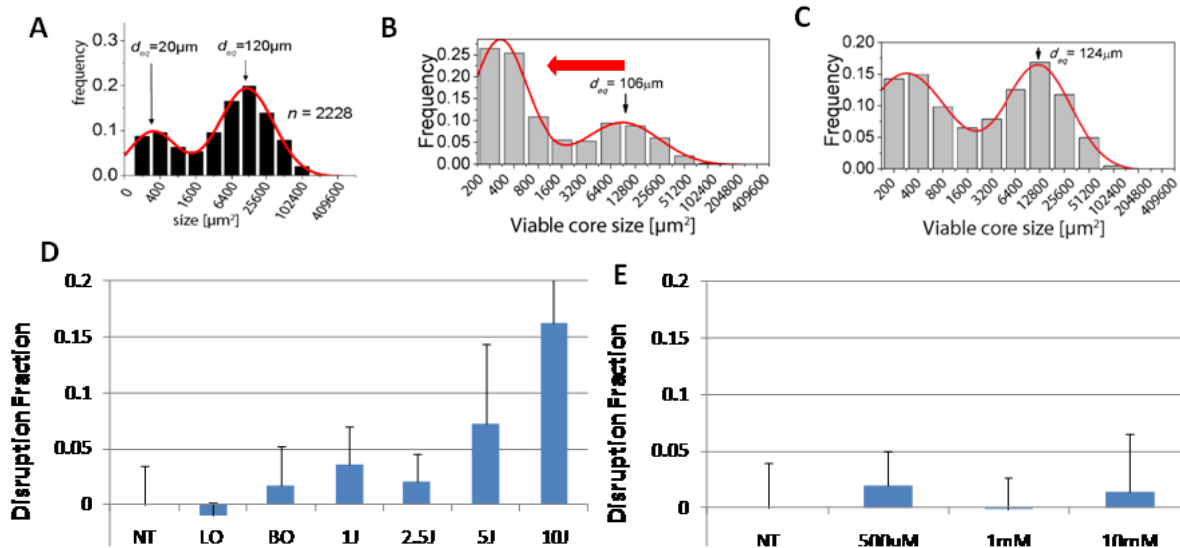
Figure 6: Quantitative analysis of size distribution of residual disease and nodular disruption following intervention. Size distributions of **A)** OvCa 3D nodules prior to treatment (day 10), **B)** following BPD-PDT treatment and **C)** following carboplatin treatment. To quantify the observation that PDT disrupts nodular structure shifting the distribution towards smaller sizes we report disruption fraction (D_{frac}) as the fractional shift from the larger size mode to the smaller mode in each bimodal lognormal distribution. As seen in **D)**, D_{frac} increases in a dose dependent manner for BPD-PDT, while in **E)**, the peripheral pattern of cyototoxic response from carbo produces negligible nodular fragmentation even at very high doses.

The data from Figures 5 and 6 suggested that there was significant fragmentation of the tumor nodules by PDT and this guidance from imaging lead us to hypothesize that the more efficient treatment outcome would be achieved by the administration of PDT first to "loosen" the tumor structure and enable the better penetration of the carboplatin which is an extremely effective agent if it reaches the target cells. Figure 7 confirms our hypothesis that the treatment with PDT first followed by carboplatin is not only more effective but also synergistic. The reverse sequence showed no such synergy.

Sequence 1: PDT before carboplatin
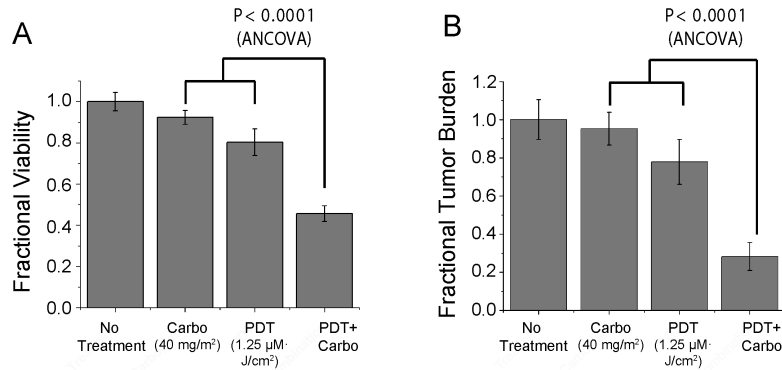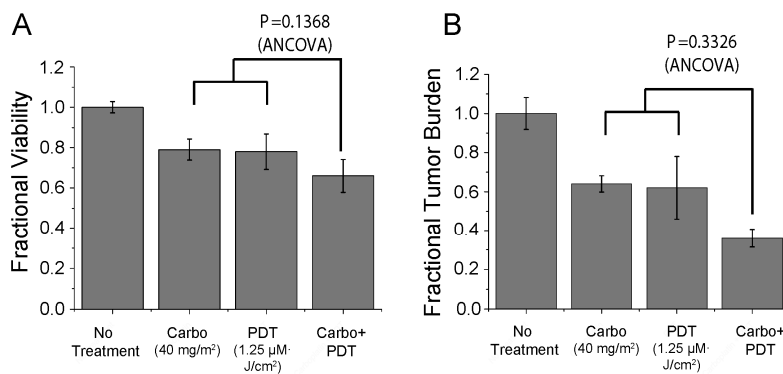

Sequence 2: Carboplatin before PDT

Figure 7: A sequence-dependent synergistic enhancement in carboplatin efficacy is observed in the 3D OvCa tumor model. Significance of the interaction was established by an analysis of co-variance (ANCOVA) statistical model previously described [12]. Here, dosage of carboplatin is calibrated to mg/m2, calculated from the concentration of carboplatin in cultures relative to the surface area of a Matrigel bed. 40mg/m^2 corresponds to a concentration of

4.   CONCLUSIONS

In summary, we have demonstrated one example of how imaging might be useful in developing therapeutic strategies. The development of a quantitative high throughput platform presented here should prove to be useful for drug discovery and for mechanistic understanding of how different drugs work. The concept of 'loosening" the tumor becomes important in many cancers such as pancreatic cancer where a major limitation is believed to be the high stromal content inhibiting drug delivery access to the cancer cells. The approach proposed here appears promising for a broader application, needs validation in animal studies and merits further development.

5.   ACKNOWLEDGEMENTS

REFERENCES

[1]   J. P. Celli, B. Q. Spring, I. Rizvi *et al.*, "Imaging and Photodynamic Therapy: Mechanisms, Monitoring, and Optimization," Chem Rev*,* 110(5), 2795-838 (2010).

[2]   D. Hanahan, and R. A. Weinberg, "The hallmarks of cancer," Cell*,* 100(1), 57-70 (2000).

[3]   B. A. Chabner, "Cytotoxic agents in the era of molecular targets and genomics," Oncologist*,* 7 Suppl 3, 34-41 (2002).

[4]   W. C. Hahn, C. M. Counter, A. S. Lundberg *et al.*, "Creation of human tumour cells with defined genetic elements," Nature*,* 400(6743), 464-8 (1999).

[5]   J. Lehar, A. S. Krueger, W. Avery *et al.*, "Synergistic drug combinations tend to improve therapeutically relevant selectivity," Nat Biotechnol*,* 27(7), 659-66 (2009).

[6]   G. R. Zimmermann, J. Lehar, and C. T. Keith, "Multi-target therapeutics: when the whole is greater than the sum of the parts," Drug Discov Today*,* 12(1-2), 34-42 (2007).

[7]   R. Agarwal, and S. B. Kaye, "Ovarian cancer: strategies for overcoming resistance to chemotherapy," Nat Rev Cancer*,* 3(7), 502-16 (2003).

[8]   T. A. Yap, C. P. Carden, and S. B. Kaye, "Beyond chemotherapy: targeted therapies in ovarian cancer," Nat Rev Cancer*,* 9(3), 167-81 (2009).

[9]   N. Ferrara, "Vascular endothelial growth factor as a target for anticancer therapy," Oncologist*,* 9 Suppl 1, 2-10 (2004).

[10]   N. Ferrara, H. Gerber, and J. LeCouter, "The biology of VEGF and its receptors," Nature Medicine*,* 9, 669-676 (2003).

[11]   J. P. Celli, I. Rizvi, C. L. Evans *et al.*, "Quantitative imaging reveals heterogeneous growth dynamics and treatment-dependent residual tumor distributions in a three-dimensional ovarian cancer model," Journal of Biomedical Optics*,* 15(5), 051603-10 (2010).

[12]   I. Rizvi, J. P. Celli, C. L. Evans *et al.*, "Synergistic Enhancement of Carboplatin Efficacy with Photodynamic Therapy in a Three-Dimensional Model for Micrometastatic Ovarian Cancer," Cancer research*,* 70(22), 9319-9328 (2010).